Articles

Nile Red Is a Fluorescent Allosteric Substrate of Cytochrome P450 3A4†

Jed N. Lampe, Cristina Fernandez, Abhinav Nath, and William M. Atkins*

Department of Medicinal Chemistry, Box 357610, University of Washington, Seattle, Washington 98195-7610

Received July 13, 2007; Revised Manuscript Received November 8, 2007

ABSTRACT: Cytochrome P450 3A4 (CYP3A4) plays a critical role in the metabolism of many drugs. CYP3A4 exhibits extraordinary substrate promiscuity and unusual allosteric kinetics. In addition, many CYPs catalyze sequential oxidations on a single substrate, but in most cases, mechanistic details of these processes are not well-established. As a result, in vivo clearance of many drugs and their metabolites is difficult to predict on the basis of the complex in vitro kinetics, and new in vitro probes are required to understand these behaviors. The near-IR fluorescent probe Nile Red, which has strong solvatochromic behavior, was investigated as a probe of allostery and sequential metabolism with CYP3A4. Nile Red binds with apparent K_d values of 0.05 and 2.3 μM, based on a sigmoidal dependence of heme spin state on Nile Red concentration, where the first equivalent of Nile Red increased the high-spin fraction by only 13% of the total change at saturation. Mass spectrometry analysis indicates that Nile Red is metabolized sequentially by CYP3A4 to the *N*-monoethyl and *N*-desethyl products, confirming that the immediate vicinity of the heme iron is one binding site. In the presence of CYP3A4, steady-state fluorescence emission and excitation spectra, as well as excited-state lifetimes at varying Nile Red concentrations, indicate a high-affinity site that modulates the fluorescent properties of Nile Red. The Nile Red binding site is competitively eliminated by itraconazole, which is a high-affinity ligand known to coordinate to the heme iron. Together, the data suggest that Nile Red binds to the active site with high affinity (∼50 nM), where it is desolvated in a low-dielectric environment. In addition, Nile Red is sequentially oxidized at rates comparable to or faster than those of other in vitro probes, which emphasizes its utility in the further examination of this important kinetic phenomenon in vitro.

Cytochrome P450's (CYPs)[1] comprise a ubiquitous superfamily of heme-containing monoxygenases that is represented in every known biological kingdom (*1*−*4*). CYPs regulate the metabolism and steady-state plasma concentrations of nearly all prescribed therapeutic drugs, as well as a number of endogenous hormones and xenobiotics (*1*, *5*, *6*). In addition, CYPs often play important roles in the biosynthesis of many pharmacologically relevant compounds in prokaryotes and plants (*1*, *2*, *4*). Their ability to perform complex oxidative metabolism on a structurally diverse set of compounds is often accompanied by complex non-Michaelis−Menten, or "allosteric", kinetics (*7*−*9*). These "atypical" kinetic profiles have been well-documented at least since the late 1980s (*10*, *11*). As described by Korzekwa and co-workers (*9*), these kinetic patterns fall into four categories: heterotropic activation, homotropic activation, substrate inhibition, and biphasic kinetics.

The predominant human hepatic drug-metabolizing CYP isoform, CYP3A4, has been studied extensively with regard to allosteric kinetic phenomena (*12*−*15*). Most models used to explain cooperativity in this enzyme have relied on the postulate that multiple ligands bind simultaneously to the enzyme (*8*, *16*, *17*), although direct confirmation of this has been challenging. Spectroscopic studies (*18*, *19*) and recently published X-ray crystal structures (*20*) have suggested that multiple-ligand binding within the CYP3A4 active site is possible. However, allosteric kinetics could be observed, even in the absence of multiple-ligand binding, if kinetically distinct conformations are not in rapid equilibrium (*21*, *22*). The available structural models emphasize the need for additional biophysical characterization of ligand binding (*20*, *23*, *24*). Although progress has been made in elucidating the biophysical basis of these complex kinetics, no single mechanistic model accounts for all of the available data. Specifically, in terms of heterotropic and homotropic activation, many questions still remain to be answered. (1) Where on the enzyme do effector ligands bind? (2) Are the binding sites overlapping, close but distinct, or spatially remote? (3) What is the mechanism by which effector ligand binding induces enzyme activation versus inhibition?

† This work was supported by NIH Grants GM32165 (W.M.A.) and GM07750 (J.N.L.).

* To whom correspondence should be addressed. E-mail: winky@u.washington.edu. Telephone: (206) 685-0379. Fax: (206) 685-3252.

[1] Abbreviations: ANF, α-naphthoflavone; CYP, cytochrome P450; EDTA, ethylenediaminetetraacetic acid; GSH, glutathione; ITZ, itraconazole; KP, potassium phosphate; KTZ, ketoconazole; MS, mass spectral; NADPH, nicotinamide adenine dinucleotide phosphate; SVD, singular-value decomposition; TNS, 2-*p*-toluidinylnaphthalene-6-sulfonic acid; TST, testosterone; UV−vis, ultraviolet−visible.

10.1021/bi7013807 CCC: $40.75
Published on Web 12/20/2007

A further complexity of CYPs, including CYP3A4, is their ability to catalyze sequential oxidation steps on a single substrate (*25*−*27*). Depending on the relative partitioning between dissociation of metabolites and forward flux toward further oxidation, the population of products in solution can have very complex time dependence and substrate concentration dependence. Therefore, probe substrates of sequential oxidation may be useful also as tools for understanding this complexity.

Previously, our lab and others have elucidated the utility of model fluorescent probes in better characterizing the location and extent of binding of effector ligand to CYP3A4 (*12*, *25*, *26*). Here, we describe the use of the previously unknown CYP3A4 fluorescent substrate Nile Red, which provides the advantage of extreme solvatochromism and which could, in principle, be used to explore the properties of any sites on CYP3A4 to which it binds. The fluorescent properties of Nile Red are likely to be useful in subsequent structure−function studies of CYP3A4.

MATERIALS AND METHODS

Chemicals. All chemicals used were analytical grade and obtained from commercial sources. Solvents were HPLC grade, and all water that was used was deionized, distilled Milli-Q quality. Nile Red was obtained from Invitrogen Corp. (Carlsbad, CA). The potassium salt of 2-*p*-toluidinylnaphthalene-6-sulfonic acid (TNS) was obtained from Marker Gene Technologies (Eugene, OR). All other chemicals used were obtained from Sigma-Aldrich (St. Louis, MO), unless otherwise noted.

Protein Expression and Purification. Recombinant CYP3A4 was expressed and purified from *Escherichia coli* as described previously, using a French press to lyse the cells (*12*). When purification was complete, the concentration of CYP3A4 was quantified by the method of Omura and Sato, using an extinction coefficient of 91 mM^{-1} cm^{-1} (*27*). The protein was judged to be greater than 95% pure by SDS−PAGE gel analysis. The purified CYP3A4 was divided into 1 mL aliquots and stored at −80 °C until further use. Each aliquot underwent no more than five freeze−thaw cycles.

Nile Red K_d Determination Using Optical Difference Spectroscopy. To quantitatively assess the nature of the binding interaction between Nile Red and CYP3A4, UV−visible difference spectra were acquired using a dual-beam OLIS/Aminco DW2a spectrophotometer (OLIS, Bogart, GA). Both the sample and reference chamber contained 1 mL of 1 μM CYP3A4 in 100 mM KP_i, 20% glycerol, and 1 mM EDTA (pH 7.4). Prior to initiation of the titration with Nile Red, a baseline was recorded between 360 and 460 nm. Subsequently, 1 μL aliquots of a 0.5 mM stock of Nile Red dissolved in acetonitrile were added to the sample cuvette while an equal volume of vehicle solvent (acetonitrile) was added to the reference cuvette. Care was taken so that the final concentration of acetonitrile in each cuvette did not exceed 1.5%. Difference spectra were acquired after a 1 min equilibration time. All spectra were recorded at 22 °C (room temperature). Data were imported into Origin version 7.5 (OriginLab Corp., Northampton, MA) for analysis. The absorbance at 360 nm of the "blank" containing Nile Red but no protein was subtracted from the spectra of samples containing protein. The absolute change in absorbance between the peaks at 425 nm and the trough at 398 nm was plotted as a function of ligand concentration. To obtain an accurate binding affinity constant, we fit the data to a variety of models, including the Hill model (*28*), and to kinetic simulations (vide infra) of a two-site random-ordered binding model that assumes the spectral change is primarily induced by the [CYP·L·L] complex instead of the [CYP·L] complex, as we previously observed for testosterone (*13*).

Reconstitution System and Kinetic Assays. Catalytic activity parameters for the CYP3A4-mediated oxidation of Nile Red were determined using a reconstituted enzyme system as described previously (*37*). Briefly, 30 pmol of purified CYP3A4, 60 pmol of rat NADPH-P450 reductase, and 30 pmol of rat cytochrome b_5 were resuspended in a buffer containing 0.1 mg/mL CHAPS, 20 μg/mL liposomes (L-α-dilauroyl-*sn*-glycerophosphocholine, L-α-dioleoyl-*sn*-glycero-3-phosphocholine, and L-α-dilauroyl-*sn*-glycero-3-phosphoserine, at a 1:1:1 weight ratio per milliliter), 600 μM GSH, and 10 mM potassium HEPES (pH 7.4). Reaction buffer and MilliQ NanoPure H_2O were added so the following final concentrations were realized: 40 mM potassium HEPES, 2.4 mM GSH, and 30 mM $MgCl_2$ (pH 7.4). This enzyme mixture was then allowed to preincubate on ice for 10 min. To determine whether Nile Red was indeed a substrate for CYP3A4, an initial incubation was conducted under the conditions described with 100 μM Nile Red for 1 h. For accurate determination of kinetic parameters, the Nile Red substrate was dissolved in acetonitrile and serially diluted to various concentrations (from 0 to 100 μM). For each substrate concentration that was tested, Nile Red was added to the enzyme mixture to a final volume of 1%. Reaction mixtures were then preincubated at 37 °C for 3 min, after which the reaction was initiated by addition of 5 μL of 1 mM NADPH. The final reaction volume was 0.5 mL. The reaction was allowed to proceed for 15 min at 37 °C, at which time the reactions were quenched by the addition of an equal volume of ethyl acetate containing TNS (2-*p*-toluidinylnaphthalene-6-sulfonic acid) as an internal standard. Metabolites were then thrice extracted with ethyl acetate and dried over $MgSO_4$ to remove excess water. The consumption of substrate at all concentrations studied was limited to less than 10%. Extracted metabolites were evaporated to dryness using a Savant SpeedVac system (GMI, Inc., Ramsey, MN). Reaction products were then dissolved in 50 μL of acetonitrile and analyzed using HPLC and HPLC−MS.

HPLC Metabolite Analysis. Metabolites produced from Nile Red by CYP3A4 were analyzed using an Agilent 1100 HPLC system (Agilent Technologies, Inc., Santa Clara, CA), equipped with an Agilent model 1100 autosampler, a ternary solvent delivery system, and a UV−vis diode array detector controlled by Agilent HPLC2D ChemStation. For analysis, 10 μL from each sample was injected onto a Zorbax SB-C18 column (5 μm, 2.1 mm × 15 mm; Agilent Technologies, Inc.) and eluted using an isocratic mobile phase consisting of a 50:50 (v/v) acetonitrile/0.1% formic acid mixture (pH 3.0) at a flow rate of 0.5 mL/min. Absorbance detection was monitored at 550 nm for 30 min. To control for internal instrument drift and extraction efficiency, TNS was used as an internal standard. Retention times of the Nile Red metabolites M2 and M1 were 2.8 and 7.7 min, respectively. Retention times of the Nile Red parent compound and of the internal standard were 22.9 and 0.8 min, respectively.

Nile red metabolites M1 and M2 were quantified by comparing the integrated peak area to an authentic standard curve produced for each metabolite. This value was then converted to picomoles per minute per picomole of CYP3A4 to yield the initial reaction velocity.

MS/MS Metabolite Identification. Metabolites were identified by electrospray LC−MS/MS analysis using a Waters Quattro II tandem quadrupole mass spectrometer (Waters, Ltd., Milford, MA) coupled to a Shimadzu (Columbia, MD) HPLC instrument. The mass spectrometer was operated in electrospray ionization mode (ESI) at a cone voltage of 45 V, a source block temperature of 100 °C, and a desolvation temperature of 350 °C. Extracts from in vitro incubations were introduced into the mass spectrometer using a Zorbax SB-C18 column (5 μm, 2.1 mm × 15 mm; Agilent Technologies, Inc.). Metabolites were eluted using an isocratic mobile phase consisting of 0.1% aqueous formic acid (solvent A) and anhydrous acetonitrile (solvent B), at a flow rate of 0.3 mL/min. Positive ions were monitored over the full-mass range of *m*/*z* 50−2000, and daughter ion spectra were generated for components of interest in selective ion monitoring mode. Data analysis was carried out using Windows NT-based Micromass MassLynxNT version 3.2.

Bioreactor Production of Authentic Nile Red Metabolites. Due to the lack of commercial availability of authentic metabolic standards, a modified bioreactor approach (*29*−*31*) was used to biosynthetically produce each metabolite for use as standards. Briefly, this approach consisted of preparing two large scale (50 mL) reactions based on the conditions described above, with each incubation containing 1 μmol of Nile Red substrate. Incubations were allowed to proceed for 1 h at 37 °C while being shaken at 150 rpm. At the end of the incubation period, metabolites M1 and M2 were extracted with ethyl acetate, as described above, and evaporated to dryness using a Büchi Rotovap 401 concentrator (Büchi Corp., New Castle, DE). Metabolites were then redissolved in 10 mL of acetonitrile and purified using a semipreparative Alltech Econosphere C-18 HPLC column (10 mm × 250 mm) with an isocratic mobile phase consisting of a 50:50 (v/v) acetonitrile/water mixture with 0.1% formic acid (pH 3.0) at a flow rate of 5 mL/min. Absorbance detection was monitored at 550 nm. For each metabolite, the peak of interest, as determined by LC−MS/MS, was collected over the course of 10 separate injections which were then separately pooled together. Pooled fractions were evaporated to dryness in oven-dried, preweighed glass vials using a Savant SpeedVac system (GMI, Inc.). The resulting solid for each metabolite (M1 and M2) was then weighed on an MT5 analytical microbalance (Mettler Toledo) using the difference method. Each metabolite was then dissolved in acetonitrile to yield a final concentration of 1 mM. An aliquot of this sample was used to generate high-resolution MS data to verify the purity of each metabolite. The standard curve was subsequently prepared from serially diluted solutions ranging from 0.24 to 500 μM.

Steady-State Fluorescence Spectroscopy. All steady-state fluorescence measurements were carried out using an 8100 SLM-Aminco spectrofluorometer with both emission and excitation monochronometers. For binding titrations with Nile Red, the excitation wavelength used was 550 nm with a bandpass of 4 nm for both monochromators. Emission spectra were acquired from 560 to 800 nm at a scan rate of 5 nm/s. For the initial titration, either a 0.5 or 1 mM stock solution of Nile Red dissolved in acetonitrile was used. The titration was carried out by sequentially adding 1 μL aliquots of the Nile Red stock solution to a 1 mL solution of 1 μM CYP3A4 diluted in 100 mM KP_i, 20% glycerol, and 1 mM EDTA (pH 7.4). Emission spectra were acquired after a 1 min equilibration period. Samples were continuously stirred during both equilibration and spectral acquisition. Care was taken so that the final concentration of acetonitrile in the cuvette did not exceed 1.5%. All spectra were recorded at 22 °C (room temperature). To determine the extent of the relative fluorescence contribution to ligand binding to each site, singular-value decomposition (SVD) was performed using an in-house SVD analysis program. Fluorescence scans at a range of ligand concentrations were assembled into a matrix, for which the Compact SVD was calculated using the linalg.svd() function of the SciPy scientific computing package (*32*) for Python.

Fluorescence Lifetime Measurements. Fluorescence lifetime measurements were conducted using a Spex Fluorolog Tau3 frequency domain spectrofluorometer with a 450 W xenon arc lamp (Horiba Jobin Yvon, Edison, NJ). For each experiment, a total of 20 frequencies were chosen, ranging from 1 to 200 MHz. Ten replicate measurements were obtained for each frequency, and the integration time for each measurement was 15 s. The excitation monochromator was set at 550 nm, and the emission monochromator was set at either 600 or 650 nm. A dilute light-scattering solution of LUDOX was used as a lifetime standard. All experiments were performed at 22 °C. Phase angle shift (φ) and modulation (*m*) decay data were fit to the simplest exponential decay model using the Model software package (Thermogalactic, Waltham, MA), according to the following intensity decay law (eq 1):

$$I(t) = \sum_{i=1}^{n} \alpha_i \exp(-\tau/\tau_i) \quad (1)$$

where α_i is the time-zero amplitude due to each specific decay time (τ_i). In terms of a single-exponential decay, the lifetime can be calculated from the phase and modulation values using

$$\tau_\varphi = \omega^{-1} \tan \varphi \quad (2)$$

$$\tau_m = \omega^{-1}\left(\frac{1}{m^2} - 1\right)^{-1/2} \quad (3)$$

where ω is the light modulation frequency in radians per second, τ_φ is the apparent phase angle shift lifetime, and τ_m is the apparent modulation lifetime. Average lifetimes (τ) of multiexponential decay were calculated using eq 4:

$$\bar{\tau} = \sum_{i=1}^{n} \frac{\alpha_i \tau_i^2}{\alpha_i \tau_i} \quad (4)$$

Kinetic Simulations. Kinetic simulations were performed using the GEPASI Biochemical Simulation Module (*33*−*35*) as described previously (*13*). Briefly, two-site random-ordered binding models were created with all bimolecular association constants fixed at 1 μM^{-1} s^{-1}. The Levenberg−

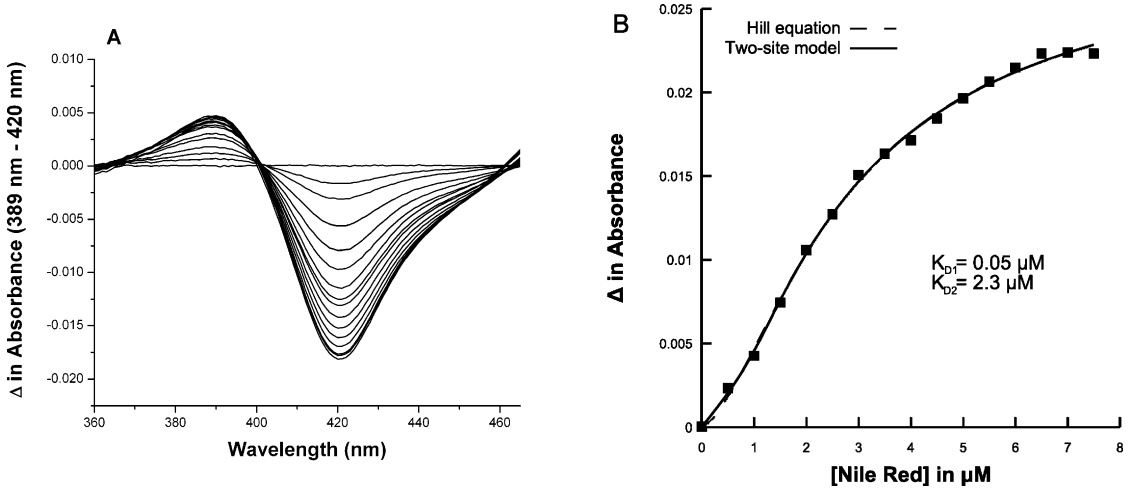

FIGURE 1: (A) UV−vis difference absorbance spectra of Nile Red binding to CYP3A4. Each spectral scan represents one 1 μL addition of 0.5 mM Nile Red. The spectra are characteristic of high-spin heme complexes of CYP3A4. (B) Binding isotherm for Nile Red binding to CYP3A4 based on the optical spectra from panel A. The difference in absorbance ($A_{389} - A_{420}$) was used, and the data were fit to both the Hill equation (dashed line) and to a sequential binding model (solid line). K_d values are shown for the sequential binding model only. The fitted lines are nearly indistinguishable.

Marquadt fitting module of GEPASI was used to vary dissociation constants and specific contributions to experimental signals (Δ in absorbance or specific fluorescence) to minimize χ^2 between observed data and simulated steady-state concentrations.

RESULTS

Spectral Equilibrium Binding Studies. To assess the utility of Nile Red as a fluorescent probe of CYP3A4−ligand interactions, we first sought to determine if it was an active site ligand of CYP3A4. To this end, we conducted an optical difference titration of Nile Red into a 1 μM solution of CYP3A4.

As seen in Figure 1A, Nile Red produces a type I difference spectra when titrated into CYP3A4. This is indicative of a low-spin to high-spin transition of the heme, suggesting displacement of the H_2O sixth axial ligand from coordination with the heme iron. Additionally, it should be noted that the effect is saturable. It is interesting to note that the binding isotherm based on the absorbance difference spectra is sigmoidal, suggestive of cooperativity at the level of ligand binding or at the level of spin-state conversion. Regardless of the detailed mechanism for apparent cooperativity in the difference spectrum, when the data were fit to the Hill equation, an S_{50} of 2.8 ± 0.14 μM and an n of 1.56 ± 0.08 were obtained (Figure 1B).

Although the S_{50} is a crude approximation of ligand affinity and not a true K_d, it suggests that Nile Red is a relatively high-affinity ligand for CYP3A4. The data were also fit to a two-site random-ordered binding model, assuming that the [E·L·L] complex, and not the [E·L] complex, primarily induces the spectral change, as we have observed previously for testosterone and more recently with α-naphthoflavone (*13*, *36*). The K_d values obtained from this model were 0.05 ± 0.1 and 2.3 ± 0.35 μM. The fractional spin-state change for the first, high-affinity, site is 13% of the total spin-state change at a saturating Nile Red concentration. Additionally, the type I spin-state shift suggested the possibility that Nile Red might also be a substrate of CYP3A4.

Kinetic Analysis of Nile Red Oxidation by CYP3A4 and Identification of Metabolites. To determine whether Nile Red was a substrate, it was incubated with CYP3A4 under standard conditions using a reconstituted assay system format (*37*). Initial incubations resulted in the formation of two major metabolites, M1 and M2, as observed by liquid chromatography with UV−vis and MS detection (Figure 2A,B).

On the basis of MS analysis, metabolites M1 (*m*/*z* 291.8) and M2 (*m*/*z* 263.8) corresponded to the loss of 28 and 56 atomic mass units from the parent compound (*m*/*z* 319.8), respectively. This is consistent with sequential N-deethylation reactions, and the individual purified products M1 and M2 are easily spectroscopically distinguishable (Figure 3).

To determine the kinetic parameters for the CYP3A4-mediated oxidation of Nile Red, bioreactor scale incubations were carried out to produce sufficient quantities of metabolites M1 and M2 for use as analytical standards. More than 1 mg of each metabolite was obtained. On the basis of these standards, the recovered velocity versus substrate concentration plot (Figure 4) for the oxidation of Nile Red to the primary metabolite M1 was hyperbolic with a K_M of 5.1 ± 0.69 μM and a V_{max} of 1.4 ± 0.07 pmol min^{-1} (pmol of CYP3A4)$^{-1}$.

The detailed mechanism of sequential metabolism, whether it is dissociative or processive, is outside the scope of this work. Further experiments will be required to determine the rate constants for individual steps with different substrate complexes.

Steady-State Fluorescence Binding Studies. As an environmentally sensitive spectroscopic probe, Nile Red provides the possibility of directly assessing binding site polarity in relation to bulk solvent and of confirming binding via spectral shifts. To probe the binding of Nile Red to CYP3A4, the fluorescence emission spectrum of Nile Red was measured as a function of ligand concentration in the presence of the protein (Figure 5).

It should be re-emphasized that Nile Red is quenched efficiently in an aqueous solvent, but it exhibits a dramatic increase in its quantum yield when bound in a hydrophobic protein or lipid environment (*38*−*44*). On the other hand, due to spectral overlap of the Nile Red emission with the weak α and β absorbance bands of the heme, FRET-

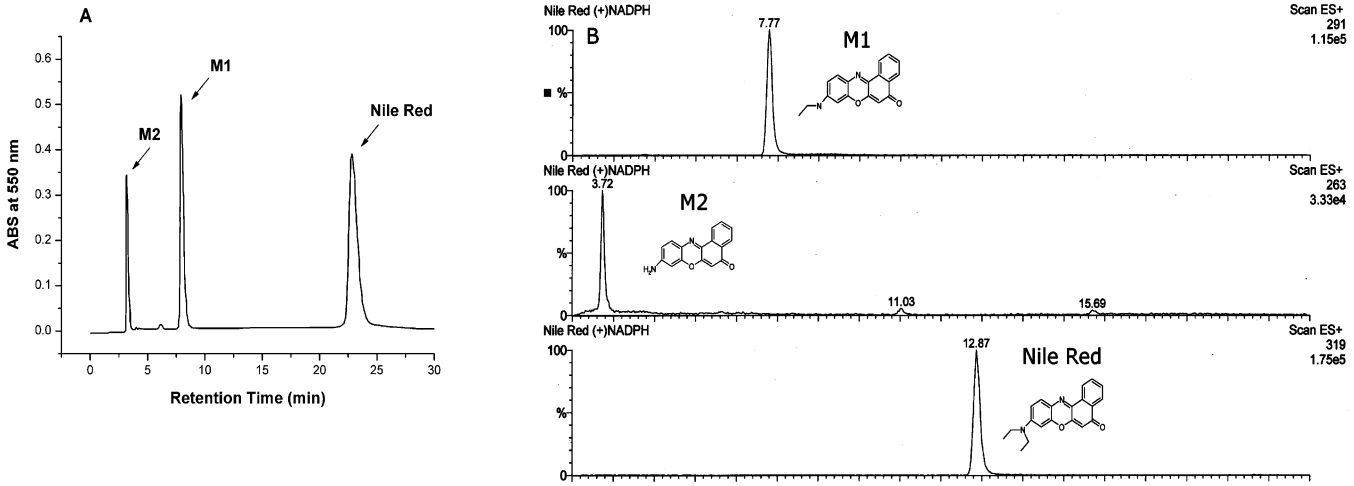

FIGURE 2: (A) HPLC chromatogram of compounds extracted after incubation of Nile Red with CYP3A4 in a reconstitution assay. Peaks M1 and M2 were tentatively assigned as metabolites of Nile Red as they were not present in the (−) NADPH control. Detection was at 550 nm. (B) Selected ion monitoring mass spectrometry for $MH^+ = 291$, $MH^+ = 263$, and $MH^+ = 319$ ions, corresponding to M1, M2, and Nile Red, respectively. Numbers above the peaks correspond to the relative retention times.

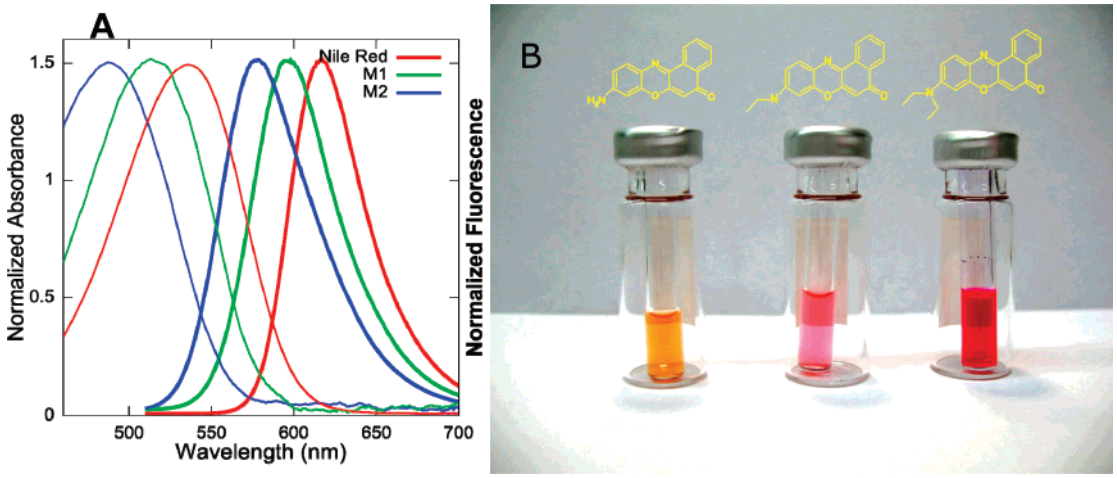

FIGURE 3: (A) Absorbance (left) and emission (right) spectra for Nile Red and its major 3A4 metabolites. (B) Nile Red and its two major metabolites, M1 and M2, dissolved in acetonitrile. Note the dramatic color change upon sequential N-dealkylations.

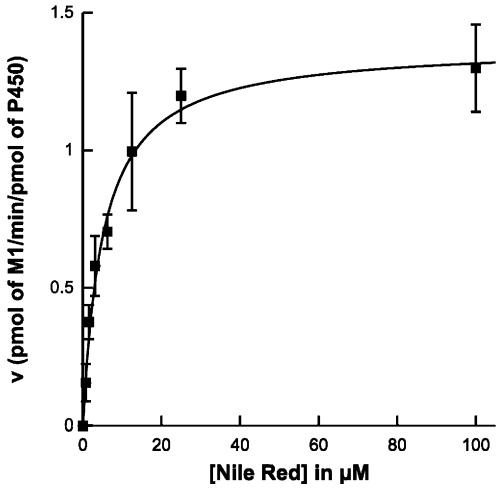

FIGURE 4: Steady-state kinetics of M1 formation. The velocity of product formation is hyperbolic with respect to Nile Red concentration.

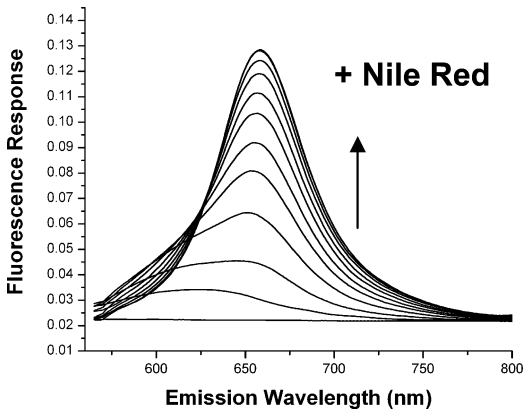

FIGURE 5: Emission spectra of increasing concentrations of Nile Red titrated into 1 μM CYP3A4. At low concentrations of Nile Red, a short-wavelength peak is observed, centered near 620 nm. With an increasing Nile Red concentration, the predominant species has a spectrum centered near 660 nm. The Nile Red concentrations that were used were 0 and 1−10 μM in 1 μM increments.

dependent quenching of the Nile Red is expected. Thus, the emission of Nile Red bound to the CYP3A4 requires detailed characterization to distinguish it from a possible contribution from free Nile Red. In Figure 5, note the appearance of an initial λ_{em} maximum at approximately 600 nm for low (<3 μM) concentrations of Nile Red bound to CYP3A4. As increasing amounts of Nile Red are added, the fluorescence increases and is dramatically red-shifted. These results

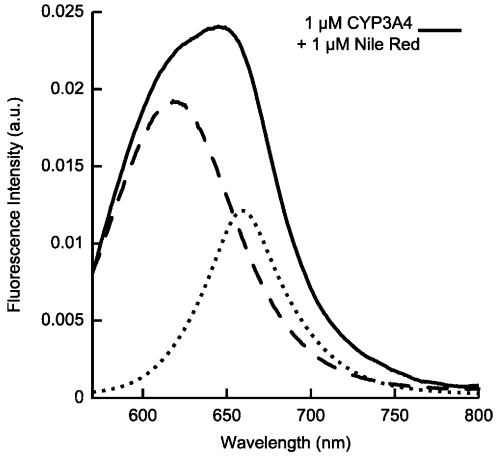

FIGURE 6: Singular-value decomposition of Nile Red emission, in the presence of CYP3A4. The experimental emission spectrum (solid line) of 1 μM CYP3A4 with 1 μM Nile Red demonstrates apparent multiple fluorescent species. The dotted line corresponds to a basis emission spectrum from SVD of Nile Red in the presence of 1 μM CYP3A4 and 2 μM itraconazole, which is sufficient to saturate the active site. The dashed line corresponds to the basis spectrum of the Nile Red bound to CYP3A4, from the residual signal remaining after subtraction of the "red basis spectrum", and it represents the apparent spectrum of Nile Red bound in the CYP3A4 active site.

suggest that there are at least two environments with different solvent accessibilities or polarities that contribute to the steady-state spectra. For convenience, we refer to these sites as the "blue" species (~620 nm) and the "red" species (~650 nm) in our subsequent discussion.

To determine whether either species represents Nile Red bound to a discrete site on the protein and to improve our understanding of this complex fluorescence behavior, we performed competition experiments with itraconazole (ITZ). ITZ is a substrate and inhibitor of CYP3A4 that forms a very high-affinity ($K_d \sim 5$ nM), low-spin complex with a coordinate bond between the lone pair electrons from an azole nitrogen ligated directly to the heme iron (*20*, *45*−*47*). In contrast to the X-ray structure obtained with a similar compound containing an azole moiety, ketoconazole (KTZ), that featured two ligand molecules simultaneously bound within the active site, we propose it is highly unlikely that multiple ITZs would be bound in our experiments. This is based on the fact that the concentration of KTZ used in the crystallographic experiment was several orders of magnitude higher than that used here (*20*). Because ITZ binds with such high affinity to the active site, any component of the emission spectrum of Nile Red bound to the CYP3A4−ITZ complex should be eliminated by ITZ. That is, ITZ provides a method of blocking the active site. The spectral results were analyzed by singular-value decomposition (SVD) to resolve the species present, by calculating "basis" spectra of the individual components that remain in the presence or absence of ITZ.

As shown in Figure 6, the fluorescent properties of Nile Red bound to CYP3A4, at low concentrations of the former, unambiguously demonstrate a blue shift due to the local protein environment. Competitive inhibition of binding to the active site by ITZ eliminates nearly completely the blue fluorescent species. The red species is more difficult to assign in terms of its "environment", because it overlaps completely with the very weak fluorescence of unbound Nile Red under our solution conditions. It is difficult to determine, therefore,

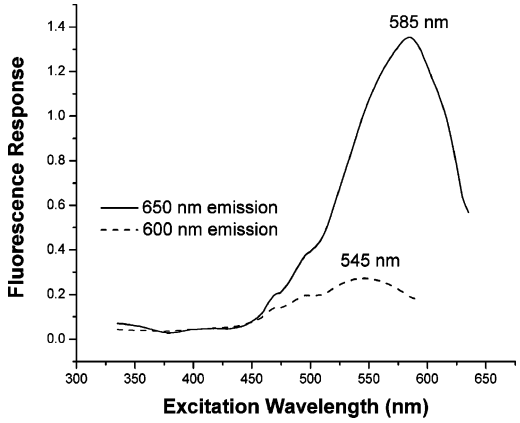

FIGURE 7: Excitation spectra of 3 μM Nile Red bound to 1 μM CYP3A4. The blue and red emission bands arise from different excitation peaks.

whether the red species is free Nile Red, Nile Red bound to a distinct site on the protein, nonspecific binding, or a combination of each of these. This is explored further in the Discussion.

The existence of two distinct fluorophore populations is also reflected in Nile Red fluorescence excitation spectra in the presence of CYP3A4 (Figure 7). At low concentrations of Nile Red, the excitation maximum is at 545 nm, whereas at higher concentrations, the maximum is at 585 nm. For excitation scans with λ_{em} at 600 nm, the fluorescence emission signal is saturated at ~3 μM Nile Red, whereas the fluorescence signal with a λ_{em} of 667 nm is not saturated until a concentration of ~8 μM Nile Red is reached. Again, both signals become red-shifted with increasing Nile Red concentrations; however, the shift is more dramatic for the 667 nm λ_{em} peak. As with emission spectra and the associated SVD, the excitation spectra indicate that the blue species is distinct from the red-shifted species, and regardless of the source of the later, the blue species most likely is due to Nile Red bound to CYP3A4.

Time-Resolved Fluorescence Spectroscopy. To further distinguish the blue and red species, and thus confirm that the former is bound to CYP3A4, frequency domain fluorescence lifetime experiments were carried out at both 600 nm (Table 1) and 650 nm emission (Table 2).

The lifetime measurements indicate the existence of more than one component of fluorescence decay for multiple concentrations of Nile Red at both wavelengths. However, the relative proportions of the individual lifetime components vary with wavelength and concentration. The two components consisted of a 1 ns lifetime and an ~3−4 ns lifetime. As one can see in Table 2, the majority of the 1 ns lifetime seems to be predominantly correlated with the 650 nm emission peak at all concentrations of Nile Red examined, whereas the longer lifetime component is more closely associated with the 600 nm emission peak (Table 1). Therefore, the main (1 ns) lifetime component is associated with the red species, while the longer (3−4 ns) lifetime component is associated with Nile Red molecules bound at the high-affinity site. Consequently, these fluorescence lifetimes are directly analogous to the steady-state contributions of the two different environments for the Nile Red ligand: a nonpolar (blue-shifted) site, where the fluorescence lifetime averages ~3.5 ns, and a more polar (red-shifted) species, where the lifetime averages ~1 ns.

Table 1: Recovered Excited-State Lifetime Parameters for Nile Red Bound to CYP3A4 at 600 nm

[Nile Red] (μM)	τ_1 (ns)	τ_2 (ns)	α_1	α_2	χ^2	τ_{ave}[a] (ns)
1	1.225 ± 0.061	4.244 ± 0.212	0.172	0.828	1.59	4.07
5	1.035 ± 0.052	4.090 ± 0.205	0.382	0.618	1.37	3.67
10	n/a[b]	n/a[b]	n/a[b]	n/a[b]	n/a[b]	n/a[b]

[a] $\bar{\tau} = \sum_i(\alpha_i\tau_i^2/\alpha_i\tau_i)$. [b] Not available.

Table 2: Recovered Excited-State Lifetime Parameters for Nile Red Bound to CYP3A4 at 650 nm

[Nile Red] (μM)	τ_1 (ns)	τ_2 (ns)	α_1	α_2	χ^2	τ_{ave}[a] (ns)
1	0.896 ± 0.044	3.197 ± 0.160	0.664	0.336	1.55	2.38
5	0.904 ± 0.045	3.175 ± 0.159	0.897	0.103	0.26	1.57
10	0.895 ± 0.045	3.210 ± 0.161	0.959	0.041	0.17	1.20

[a] $\bar{\tau} = \sum_i(\alpha_i\tau_i^2/\alpha_i\tau_i)$.

DISCUSSION

Fluorescence spectroscopy has been successfully exploited by several labs to probe the various putative binding sites of CYP3A4 (*12*, *14*, *18*, *19*, *25*, *43*, *48*). Some studies have utilized heme-dependent quenching of fluorophores to assess ligand binding and to monitor putative conformational changes (*26*, *48*). In those cases, as the probe binds to the enzyme, or as a conformational change favors FRET with the heme, its fluorescence spectrum is eliminated or decreased. Here, we demonstrate the utility of an alternative case with Nile Red, wherein the probe exhibits fluorescence when it is bound to the protein that is distinct from any contribution from Nile Red in solution. This allows fluorescence spectra to be recorded when the ligand is bound to the protein, without complete heme-dependent quenching or spectral overlap, similar to our previous studies with the fluorophore TNS (*12*).

In addition, the data suggest the possibility that Nile Red binds to CYP3A4 with a stoichiometry higher than 1:1. This is based on the sigmoidal binding isotherm obtained when the spin-state equilibrium is monitored as a function of Nile Red concentration (Figure 1). At least one location for Nile Red must be the active site, inasmuch as it is also a substrate, which further adds to the utility of Nile Red as a probe of CYP3A4. Interestingly, however, the catalytic studies yield a hypberbolic velocity versus Nile Red concentration plot. This suggests that the first Nile Red and subsequent Nile Red molecules differentially perturb the heme spin state but they do not yield CYP complexes with different kinetic parameters, at least within the resolution of the assay.

An unknown aspect of our results concerns the possibility that the red species includes a component of Nile Red bound in a second site on the protein. Because free Nile Red emits weakly in aqueous solution with the same wavelength maximum as the red species we observe, further experiments are required to address this possibility. As noted above, FRET from Nile Red to the heme is expected to limit its emission intensity when bound to CYP3A4. On the other hand, the blue species demonstrates the possibility that FRET would not necessarily eliminate all Nile Red emission. Speculatively, the observed red species includes a contribution from Nile Red bound at a low-affinity site, and this could be related to the sigmoidal binding curve observed in Figure 1. However, additional studies are required to quantify this putative binding site.

As an extension of these results, it is interesting to speculate also that other fluorophores may be metabolized to products with distinct excitation and emission properties, as with M1 and M2. In this manner, CYP3A4 might be used "biosynthetically" to generate new fluorophores. Many in vitro assays utilize differential fluorescence properties of substrate and product to measure catalytic activity; however, there are not many examples of the use of CYPs as catalysts to prepare new fluorescent probes. In summary, we have introduced a new fluorescent substrate of CYP3A4 that undergoes sequential oxidation and exhibits complex binding behavior. Further characterization of the sequential metabolism of Nile Red in the presence and absence of various effector molecules may shed additional light on the allosteric mechanisms of this important enzyme.

ACKNOWLEDGMENT

We thank Drs. Timothy Schulz-Utermoehl (Merck, UK) and Matt McDonald (University of Washington) for their helpful advice regarding HPLC-MS conditions and reconstitution procedures.

REFERENCES

1. Ortiz de Montellano, P. R. (2005) *Cytochrome P450: Structure, Mechanism, and Biochemistry*, 3rd ed., Kluwer Academic/Plenum Publishers, New York.
2. Guengerich, F. P. (2002) Cytochrome P450 enzymes in the generation of commercial products, *Nat. Rev. Drug Discovery 1*, 359−366.
3. Verras, A., and Ortiz de Montellano, P. R. (2006) Protein dynamics and imidazole binding in cytochrome P450 enzymes, *Biochem. Soc. Trans. 34*, 1170−1172.
4. Johnson, E. F., and Stout, C. D. (2005) Structural diversity of human xenobiotic-metabolizing cytochrome P450 monooxygenases, *Biochem. Biophys. Res. Commun. 338*, 331−336.
5. Guengerich, F. P. (2006) Cytochrome P450s and other enzymes in drug metabolism and toxicity, *AAPS J. 8*, E101−E111.
6. Atkins, W. M. (2005) Non-Michaelis-Menten kinetics in cytochrome P450-catalyzed reactions, *Annu. Rev. Pharmacol. Toxicol. 45*, 291−310.
7. Shou, M. (2004) The impact of cytochrome P450 allosterism on pharmacokinetics and drug-drug interactions, *Drug Discovery Today 9*, 636−637.
8. Shou, M., Grogan, J., Mancewicz, J. A., Krausz, K. W., Gonzalez, F. J., Gelboin, H. V., and Korzekwa, K. R. (1994) Activation of CYP3A4: Evidence for the simultaneous binding of two substrates in a cytochrome P450 active site, *Biochemistry 33*, 6450−6455.
9. Korzekwa, K. R., Krishnamachary, N., Shou, M., Ogai, A., Parise, R. A., Rettie, A. E., Gonzalez, F. J., and Tracy, T. S. (1998) Evaluation of atypical cytochrome P450 kinetics with two-substrate models: Evidence that multiple substrates can simultaneously bind to cytochrome P450 active sites, *Biochemistry 37*, 4137−4147.

10. Wrighton, S. A., Campanile, C., Thomas, P. E., Maines, S. L., Watkins, P. B., Parker, G., Mendez-Picon, G., Haniu, M., Shively, J. E., Levin, W., et al. (1986) Identification of a human liver cytochrome P-450 homologous to the major isosafrole-inducible cytochrome P-450 in the rat, *Mol. Pharmacol. 29*, 405−410.
11. Schwab, G. E., Raucy, J. L., and Johnson, E. F. (1988) Modulation of rabbit and human hepatic cytochrome P-450-catalyzed steroid hydroxylations by α-naphthoflavone, *Mol. Pharmacol. 33*, 493−499.
12. Lampe, J. N., and Atkins, W. M. (2006) Time-resolved fluorescence studies of heterotropic ligand binding to cytochrome P450 3A4, *Biochemistry 45*, 12204−12215.
13. Roberts, A. G., Campbell, A. P., and Atkins, W. M. (2005) The thermodynamic landscape of testosterone binding to cytochrome P450 3A4: Ligand binding and spin state equilibria, *Biochemistry 44*, 1353−1366.
14. Tsalkova, T. N., Davydova, N. Y., Halpert, J. R., and Davydov, D. R. (2007) Mechanism of interactions of α-naphthoflavone with cytochrome P450 3A4 explored with an engineered enzyme bearing a fluorescent probe, *Biochemistry 46*, 106−119.
15. Isin, E. M., and Guengerich, F. P. (2006) Kinetics and thermodynamics of ligand binding by cytochrome P450 3A4, *J. Biol. Chem. 281*, 9127−9136.
16. Shou, M., Dai, R., Cui, D., Korzekwa, K. R., Baillie, T. A., and Rushmore, T. H. (2001) A kinetic model for the metabolic interaction of two substrates at the active site of cytochrome P450 3A4, *J. Biol. Chem. 276*, 2256−2262.
17. Denisov, I. G., Baas, B. J., Grinkova, Y. V., and Sligar, S. G. (2007) Cooperativity in cytochrome P450 3A4: Linkages in substrate binding, spin state, uncoupling, and product formation, *J. Biol. Chem. 282*, 7066−7076.
18. Dabrowski, M. J., Schrag, M. L., Wienkers, L. C., and Atkins, W. M. (2002) Pyrene•pyrene complexes at the active site of cytochrome P450 3A4: Evidence for a multiple substrate binding site, *J. Am. Chem. Soc. 124*, 11866−11867.
19. Khan, K. K., Liu, H., and Halpert, J. R. (2003) Homotropic versus heterotopic cooperativity of cytochrome P450eryF: A substrate oxidation and spectral titration study, *Drug Metab. Dispos. 31*, 356−359.
20. Ekroos, M., and Sjogren, T. (2006) Structural basis for ligand promiscuity in cytochrome P450 3A4, *Proc. Natl. Acad. Sci. U.S.A. 103*, 13682−13687.
21. Koley, A. P., Buters, J. T., Robinson, R. C., Markowitz, A., and Friedman, F. K. (1995) CO binding kinetics of human cytochrome P450 3A4. Specific interaction of substrates with kinetically distinguishable conformers, *J. Biol. Chem. 270*, 5014−5018.
22. Davydov, D. R., Halpert, J. R., Renaud, J. P., and Hui Bon Hoa, G. (2003) Conformational heterogeneity of cytochrome P450 3A4 revealed by high pressure spectroscopy, *Biochem. Biophys. Res. Commun. 312*, 121−130.
23. Williams, P. A., Cosme, J., Vinkovic, D. M., Ward, A., Angove, H. C., Day, P. J., Vonrhein, C., Tickle, I. J., and Jhoti, H. (2004) Crystal structures of human cytochrome P450 3A4 bound to metyrapone and progesterone, *Science 305*, 683−686.
24. He, Y. A., Gajiwala, K. S., Wu, M., Parge, H., Burke, B., Lee, C. A., and Wester, M. R. (2006) The crystal structure of human CYP3A4 in complex with testosterone, in *Abstracts, 16th International Symposium on Microsomal Drug Oxidations (MDO 2006)*, p 114, Diamond Congress, Ltd., Budapest, Hungary.
25. Fernando, H., Halpert, J. R., and Davydov, D. R. (2006) Resolution of multiple substrate binding sites in cytochrome P450 3A4: The stoichiometry of the enzyme-substrate complexes probed by FRET and Job's titration, *Biochemistry 45*, 4199−4209.
26. Stortelder, A., Keizers, P. H., Oostenbrink, C., De Graaf, C., De Kruijf, P., Vermeulen, N. P., Gooijer, C., Commandeur, J. N., and Van der Zwan, G. (2006) Binding of 7-methoxy-4-(aminomethyl)-coumarin to wild-type and W128F mutant cytochrome P450 2D6 studied by time-resolved fluorescence spectroscopy, *Biochem. J. 393*, 635−643.
27. Omura, T., and Sato, R. (1962) A new cytochrome in liver microsomes, *J. Biol. Chem. 237*, 1375−1376.
28. Hill, A. V. (1913) XLVII. The combinations of haemoglobin with oxygen and with carbon monoxide, *Biochem. J. 7*, 471−480.
29. Rushmore, T. H., Reider, P. J., Slaughter, D., Assang, C., and Shou, M. (2000) Bioreactor systems in drug metabolism: Synthesis of cytochrome P450-generated metabolites, *Metab. Eng. 2*, 115−125.
30. Otey, C. R., Bandara, G., Lalonde, J., Takahashi, K., and Arnold, F. H. (2006) Preparation of human metabolites of propranolol using laboratory-evolved bacterial cytochromes P450, *Biotechnol. Bioeng. 93*, 494−499.
31. Parikh, A., Gillam, E. M., and Guengerich, F. P. (1997) Drug metabolism by *Escherichia coli* expressing human cytochromes P450, *Nat. Biotechnol. 15*, 784−788.
32. Jones, E., Oliphant, T., Peterson P., et al. (2001) *SciPy: Open Source Scientific Tools for Python*.
33. Mendes, P. (1993) GEPASI: A software package for modelling the dynamics, steady states and control of biochemical and other systems, *Comput. Appl. Biosci. 9*, 563−571.
34. Mendes, P. (1997) Biochemistry by numbers: Simulation of biochemical pathways with Gepasi 3, *Trends Biochem. Sci. 22*, 361−363.
35. Mendes, P., and Kell, D. (1998) Non-linear optimization of biochemical pathways: Applications to metabolic engineering and parameter estimation, *Bioinformatics 14*, 869−883.
36. Roberts, A. G., and Atkins, W. M. (2007) Energetics of heterotropic cooperativity between α-naphthoflavone and testosterone binding to CYP3A4, *Arch. Biochem. Biophys.* (in press).
37. Shaw, P. M., Hosea, N. A., Thompson, D. V., Lenius, J. M., and Guengerich, F. P. (1997) Reconstitution premixes for assays using purified recombinant human cytochrome P450, NADPH-cytochrome P450 reductase, and cytochrome b5, *Arch. Biochem. Biophys. 348*, 107−115.
38. Sackett, D. L., and Wolff, J. (1987) Nile red as a polarity-sensitive fluorescent probe of hydrophobic protein surfaces, *Anal. Biochem. 167*, 228−234.
39. Ruvinov, S. B., Yang, X. J., Parris, K. D., Banik, U., Ahmed, S. A., Miles, E. W., and Sackett, D. L. (1995) Ligand-mediated changes in the tryptophan synthase indole tunnel probed by nile red fluorescence with wild type, mutant, and chemically modified enzymes, *J. Biol. Chem. 270*, 6357−6369.
40. Brown, M. B., Miller, J. N., and Seare, N. J. (1995) An investigation of the use of nile red as a long-wavelength fluorescent probe for the study of α1-acid glycoprotein-drug interactions, *J. Pharm. Biomed. Anal. 13*, 1011−1017.
41. Santra, M. K., Banerjee, A., Krishnakumar, S. S., Rahaman, O., and Panda, D. (2004) Multiple-probe analysis of folding and unfolding pathways of human serum albumin. Evidence for a framework mechanism of folding, *Eur. J. Biochem. 271*, 1789−1797.
42. Polverini, E., Cugini, G., Annoni, F., Abbruzzetti, S., Viappiani, C., and Gensch, T. (2006) Molten globule formation in apomyoglobin monitored by the fluorescent probe Nile Red, *Biochemistry 45*, 5111−5121.
43. Hungerford, G., Rei, A., and Ferreira, M. I. (2005) Studies on the interaction of Nile red with horseradish peroxidase in solution, *FEBS J. 272*, 6161−6169.
44. Sackett, D. L., Knutson, J. R., and Wolff, J. (1990) Hydrophobic surfaces of tubulin probed by time-resolved and steady-state fluorescence of nile red, *J. Biol. Chem. 265*, 14899−14906.
45. Pearson, J. T., Hill, J. J., Swank, J., Isoherranen, N., Kunze, K. L., and Atkins, W. M. (2006) Surface plasmon resonance analysis of antifungal azoles binding to CYP3A4 with kinetic resolution of multiple binding orientations, *Biochemistry 45*, 6341−6353.
46. Kunze, K. L., Nelson, W. L., Kharasch, E. D., Thummel, K. E., and Isoherranen, N. (2006) Stereochemical aspects of itraconazole metabolism in vitro and in vivo, *Drug Metab. Dispos. 34*, 583−590.
47. Locuson, C. W., Hutzler, J. M., and Tracy, T. S. (2007) Visible spectra of type II cytochrome P450-drug complexes: Evidence that "incomplete" heme coordination is common, *Drug Metab. Dispos. 35*, 614−622.
48. Fernando, H., Halpert, J. R., and Davydov, D. R. (2006) Resolution of multiple substrate bindingsites in cytochrome P450 3A4: The stoichiometry of the enzyme-substrate complexes probed by FRET and Job's titration, *Biochemistry 45*, 4199−4209.

BI7013807